JOURNAL OF AIRCRAFT
Vol. 32, No. 1, January–February 1995

Flutter Suppression for the Active Flexible Wing: A Classical Design

M. R. Waszak*
NASA Langley Research Center, Hampton, Virginia 23665
and
S. Srinathkumar†
National Aeronautical Laboratory, Bangalore 560017, India

The synthesis and experimental validation of a control law for an active flutter suppression system for the active flexible wing wind-tunnel model is presented. The design was accomplished with traditional root locus methods making extensive use of interactive computer graphics tools and simulation-based analysis. The design approach relied on a fundamental understanding of the flutter mechanism to formulate a very simple control law structure resulting in a filter with a "inverted notch" characteristic. This unusual filter characteristic was required to compensate for adverse zero locations in the frequency range near flutter. Wind-tunnel tests of the flutter suppression controller demonstrated simultaneous suppression of two flutter modes, significantly increasing the flutter dynamic pressure. The flutter suppression controller was also successfully operated in combination with a rolling maneuver controller to perform flutter suppression during rapid rolling maneuvers.

Introduction

MODERN aircraft designs emphasize the reduction of structural weight to maximize efficiency and agility. Reduced structural weight, however, can result in reduced stiffness. It is the goal of the active flexible wing[1] concept to exploit reduced stiffness to enhance maneuverability. A consequence of employing the active flexible concept may be the increased likelihood of structural dynamic instabilities (flutter). Active flutter suppression is a possible solution to this problem. Developing methods to suppress flutter by utilizing active control systems was an objective of the active flexible wing (AFW) program.[2]

Active flutter suppression has been demonstrated many times in the past,[3–11] but few studies have addressed violent clean-wing flutter of the type demonstrated by the AFW. In most cases, the control laws used to suppress flutter have relied on a single control surface and either one or two sensors (typically accelerometers). The implication is that flutter suppression does not generally require complex multivariable control. Although an objective of the AFW program was to use multivariable control methods to design the active flutter suppression system (FSS), the authors found that classical methods were sufficient. In fact, the classically designed controller described herein had the same level of performance as the other designs that relied on multivariable optimization-based methods.[12,13] In addition, the classical design was completed well in advance of the other designs and succeeded in meeting the program objectives the first time the loop was closed, without any modifications once the wind-tunnel tests began. Other control laws required extensive redesigns and modifications after the initiation of the wind-tunnel tests, and in their final form were essentially single-input/single-output.[12,13] An important requirement for flutter suppression to gain acceptance is the ability to work the first time, and every time without the need for extensive tuning or redesigning after the first flight. The success of the design presented herein is a step toward meeting that requirement.

This article focuses on the design and wind-tunnel test of a classical control law for the AFW FSS. The operation of the flutter suppression controller with the AFW wind-tunnel model in a fixed, wings-level attitude and while performing rapid rolling maneuvers are specifically addressed. Emphasis is placed on developing an understanding of the fundamental dynamic characteristics of the flutter mechanism that is crucial in the design of a successful FSS, regardless of the control law synthesis approach used. This understanding was developed using traditional graphical analysis tools. Classical methods are also used to design the feedback in a manner that stabilizes the flutter mode without otherwise adversely affecting the basic dynamic properties of the wind-tunnel model and without undue complexity. Additional discussion of the design and validation of the control laws described herein are presented in Refs. 14–17.

Experimental Facilities

The AFW wind-tunnel model was an actively controlled, statically and aeroelastically scaled, full-span wind-tunnel model of an advanced fighter aircraft. The vehicle was supported by a sting with a ball bearing and brake mechanism that allowed the vehicle to be fixed- or free-to-roll about the sting axis. Three control surfaces, controlled by hydraulic actuators and located on each wing semispan, were available for suppressing flutter: leading-edge outboard (LEO), trailing-edge outboard (TEO), and trailing-edge inboard (TEI). Four accelerometers were located on each wing semispan. Three of the accelerometers were located near the hingelines of the LEO, TEO, and TEI control surfaces near the surface midspan, and one was located near the wingtip at about midchord. A photograph and more detailed description of the wind-tunnel model is presented in Ref. 2.

The active flutter suppression control law was implemented on a digital computer running at 200 samples/s. Analog measurement signals were prefiltered by a first-order, 25-Hz antialiasing filter and could also be passed through notch filters. Separate channels were used to control flutter and the rolling

Received May 10, 1992; revision received March 7, 1994; accepted for publication March 21, 1994.

*Aerospace Research Engineer. Senior Member AIAA.
†Senior National Research Council Associate; currently Division Head, Flight Mechanics and Controls, P.B. 1779.

maneuver. Since there are two distinct flutter modes (one symmetric and one antisymmetric), a separate channel was used to control each flutter mode. A detailed description of the digital controller is presented in Ref. 18. The controller architecture could not be modified by the control law designer other than to specify characteristics of the analog notch filters.

The wind-tunnel model and digital controller were tested during two wind-tunnel entries. These tests were performed in the NASA Langley Transonic Dynamics Tunnel (TDT).[2] The operating conditions were limited to low subsonic speeds (<Mach 0.5) at atmospheric pressure. Dynamic pressure was varied over a range from 0 to approximately 300 psf.

Mathematical Model

A high-fidelity simulation model of the AFW wind-tunnel model was used for control law synthesis and analysis. It consisted of representations of structural and aerodynamic characteristics, control surface actuator dynamics, wind-tunnel turbulence, and digital controller dynamics. Linear equations of motion for the structural dynamics, unsteady aerodynamics, and controller dynamics were used, and nonlinearities such as control surface deflection limits, actuator rate limits, and quantization effects were characterized. The effects of wind-tunnel turbulence were incorporated into the model using a Dryden spectrum representation. A detailed description of the mathematical model can be found in Refs. 15, 19, and 20.

Linear models, used extensively in the control system design and analysis process, were obtained by linearizing the nonlinear model about equilibrium points at various operating conditions. In all, there were 22 linear models used: 11 models each for the symmetric and antisymmetric flutter modes, obtained at each of 11 dynamic pressures from 100 to 350 psf, in intervals of 25 psf. Each linear model had 79 states: 60 aircraft states (10 modes with 4 aerodynamic lag states per mode),[21] 9 actuator states (three third-order actuators), 2 Dryden gust states,[15] 4 antialiasing filter states (one for each accelerometer channel), and 4 delay states (digital time delay was represented by a first-order Pade approximation in each accelerometer channel).

Flutter Mechanism

When fixed-in-roll, the AFW wind-tunnel model exhibited two distinct classical bending/torsion flutter modes[22] (symmetric and antisymmetric) within the operating range of the wind tunnel. There were striking similarities between the symmetric and antisymmetric flutter mechanisms. These are evident by comparing the root loci associated with the two flutter modes,[16] and by the similarities in the predicted flutter frequencies (symmetric—11.2 Hz, antisymmetric—10.9 Hz) and flutter dynamic pressures (symmetric—248 psf, antisymmetric—233 psf). These similarities were exploited in the control law design.

The predicted symmetric dynamic characteristics of the AFW wind-tunnel model are represented by the dynamic pressure root loci presented in Figs. 1 and 2. The root loci describe the pole and zero locations with variations in dynamic pressure of the open-loop transfer function associated with symmetric tip accelerometer response due to TEO actuator commands. The symmetric loci are the same regardless of whether the model is fixed-in-roll or free-to-roll. The dynamic pressure root loci for other sensor/actuator pairs have similar characteristics. The antisymmetric dynamic pressure loci also have similar characteristics and are shown in Ref. 16. Figure 1 depicts the loci of the poles and zeros associated with the symmetric aeroelastic modes, unsteady aerodynamic lags, actuator dynamics, antialiasing filters, and time delay representations contained in the model. Figure 2 depicts a close-up of the region containing the poles and zeros associated with the flutter mechanism.

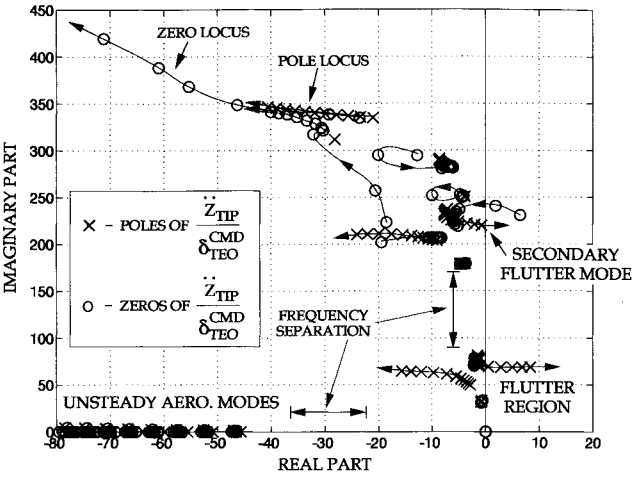

Fig. 1 Symmetric dynamic pressure root loci: open-loop (dynamic pressure range: 100–350 psf, 25-psf intervals).

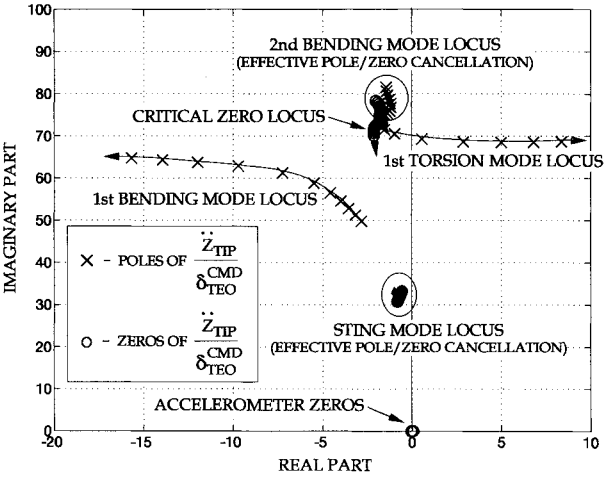

Fig. 2 Close-up of symmetric dynamic pressure root loci: open-loop (dynamic pressure range: 100–350 psf, 25-psf intervals).

Understanding the characteristics of the root loci in Figs. 1 and 2 plays a key role in suppressing the flutter modes. The locations of many of the poles and zeros vary widely over the range of dynamic pressures while others remain relatively fixed. The blurry loci correspond to these slowly migrating poles and zeros and are typically associated with near cancellations between poles and zeros in close proximity, this is pointed out in Fig. 2. The location of these poles cannot generally be appreciably altered with feedback.

A distinct frequency separation occurs between the modes associated with the flutter mechanism and the modes associated with higher frequency structural modes and unsteady aerodynamics. The frequency separation implies that an FSS could be designed to stabilize the flutter modes without significantly affecting, or being affected by, higher-order dynamics. It is only the poles and zeros in the frequency range near the flutter mode that directly affect the control law design, assuming that it rolls off at frequencies above the flutter frequency.

The most important and unique characteristic of the root loci for the AFW relates to the location of the zero locus near the first torsion mode in Fig. 2. This zero locus appears in approximately the same location for both the symmetric and antisymmetric flutter modes and for each sensor/control surface pair, and so cannot be avoided. As will be discussed below, a zero in this position introduces gain requirements that cannot be met using filter structures like those used in previous studies.[3–5,9–11] These zeros are called the "critical zeros" in the remainder of this article.

Control Law Development

The primary performance objective of the flutter suppression control law was to maintain stability over the range of dynamic pressures that were anticipated during the wind-tunnel tests (0–300 psf) subject to the disturbances associated with nominal wind-tunnel turbulence. An additional objective was to perform flutter suppression while simultaneously performing rapid rolling maneuvers. This required the concurrent operation of both an FSS controller and a rolling maneuver controller.

Gain and phase margin specifications of ± 4 dB and ± 30 deg, respectively, were selected to reflect required levels of robustness over the operating range to account for modeling errors and uncertainties. To reduce the probability of actuator rate limiting, the rms commanded actuator rate was required to be less than 50 deg/s, one-third the maximum achievable rate. Since the controller was designed to operate at a sampling rate of 200 Hz, all required computations had to be completed in approximately half of the sample period of 0.005 s.[18]

The basic design philosophy for the FSS control law was to devise the simplest control law structure that met all the design objectives. A low complexity control law increases the likelihood of meeting computational requirements, simplifies the process of verifying the correct implementation, and greatly simplifies the process of identifying the source and remedy of problems should they occur. This is possible because the designer retains the ability to readily identify the relationships between the open-loop system dynamics and the effects of feedback. This approach also reduced the time needed to develop the basic control law and permitted extensive analysis of the system performance and robustness.

The design approach was to reduce the number of sensors and control surfaces used to suppress the flutter and identify a simple compensation strategy to satisfy the design specifications. Only the control surfaces that were most effective in controlling the flutter modes and the sensors most able to sense the flutter motions were chosen. Analysis of the static control effectiveness predicted by the mathematical models indicated that the TEI and TEO surfaces were much more effective in controlling both symmetric and antisymmetric flutter than the leading-edge surface. The TEO surfaces were utilized for suppressing the symmetric flutter mode, and the two pairs of trailing-edge surfaces (TEO and TEI) were utilized for suppressing the antisymmetric flutter mode.

The predicted accelerometer characteristics were such that, although each accelerometer was fairly responsive to the flutter modes, only the wingtip accelerometer was relatively insensitive to the higher frequency modes. This can be seen in the power spectrum plot of the tip accelerometer response to turbulence shown in Ref. 23. The LEO, TEI, and TEO accelerometers required additional filtering to generate the required high-frequency rolloff. The phase lags and the added complexity associated with additional filtering were deemed undesirable. As a result, the wingtip accelerometer $\ddot{z}_{\mathrm{TIP}}$ was the only sensor used in the design.

The control law synthesis process was similar to that used by Schmidt and Chen.[11] The basic tools used in the FSS design process were root locus and Nyquist plots. The control law was designed as a continuous time system and discretized using the Tustin transformation. The discretization process is described in Ref. 15.

The open-loop dynamic pressure root loci for the wingtip acceleration due to TEO surface deflection (Fig. 2) reveals that the flutter mechanism depended primarily on two structural modes, the first bending mode and first torsion mode. These modes, the critical zeros, and the two zeros at the origin associated with the use of acceleration feedback were all that was required to effectively characterize the flutter mechanism. The two additional modes in the same frequency range (sting mode and second bending mode) had little influence since, for the chosen sensor/control surface combination, there were near pole-zero cancellations associated with these modes (this was the case for other sensors and control surfaces as well).

The positions of the critical zeros close to the imaginary axis play a key role in determining whether feedback is stabilizing or not and are responsible for a relatively large gain required to stabilize the system using constant gain feedback. Since the poles and zeros are uncertain and migrate with changes in dynamic pressure, it is important that feedback be stabilizing for a wide range of possible pole and zero locations. The large gain required for stabilization is undesirable due to its effect on higher frequency dynamics that can cause higher frequency poles to become unstable.

The frequency separation between the flutter region and the other dynamics and bandwidth limitations of the actuators required that the higher-order dynamics be accommodated by providing sufficient gain attenuation to avoid exciting them. With the possible exception of the secondary flutter mode associated with the symmetric motion (see Fig. 1), the higher frequency modes exhibited sufficient damping over the entire range of dynamic pressures so that no control action was needed. The frequency of the secondary symmetric flutter mode was outside the bandwidth of the available actuators, and the predicted flutter dynamic pressure was outside the operating range of the TDT. The best course of action for this case was also to avoid exciting these dynamics, and so minimize the possibility of reducing the dynamic pressure at which instability occurs.

Compensation elements were required to assure that the flutter was stabilized when subject to plant variations and modeling errors, and that the feedback gain could be small enough to assure that high-frequency poles remain stable. This was accomplished using root locus concepts to develop a simple third-order filter structure characterized by a pair of complex conjugate poles near the critical zeros, a pair of highly damped complex conjugate zeros, and a first-order washout filter.

A washout filter pole was chosen to assure that undesired low-frequency disturbances and measurement biases were attenuated. Complex conjugate poles were placed in locations near, but clearly to the left of, the critical zero loci. This assured that the resulting pole-zero interaction resulted in stabilizing the flutter mode over the entire range of dynamic pressures (both below and above the flutter dynamic pressure), even when subjected to moderate modeling errors. The complex conjugate zeros were chosen to simultaneously maximize the gain and phase margins of the system over the range of dynamic pressures. The gain values were chosen to equalize the positive and negative gain margins over the range of dynamic pressures. Gain scheduling could potentially have been used to improve performance and robustness at each dynamic pressure, but the complexity this introduced was deemed unacceptable, and so a single gain value was used at all dynamic pressures. The transfer function used in the flutter suppression control laws is

$$K(s) = 0.4871 \frac{s}{s+5} \frac{(s+40+j75)(s+40-j75)}{(s+7+j70)(s+7-j70)}$$

A frequency response plot of this filter is shown in Fig. 3. Note that the control law resembles an inverted notch filter since it amplifies signals over a narrow frequency range. This characteristic allowed the unstable plant pole to be stabilized over the whole range of dynamic pressures with a gain sufficiently small that higher-order plant dynamics were not significantly affected. Note also that there is no rolloff in the filter. This characteristic was acceptable because the desired rolloff is provided by the first-order, 25-Hz antialiasing filter, and by the high-frequency attenuation associated with the tip accelerometer response. The added rolloff afforded by the antialiasing filter is superimposed on the filter frequency response in Fig. 3.

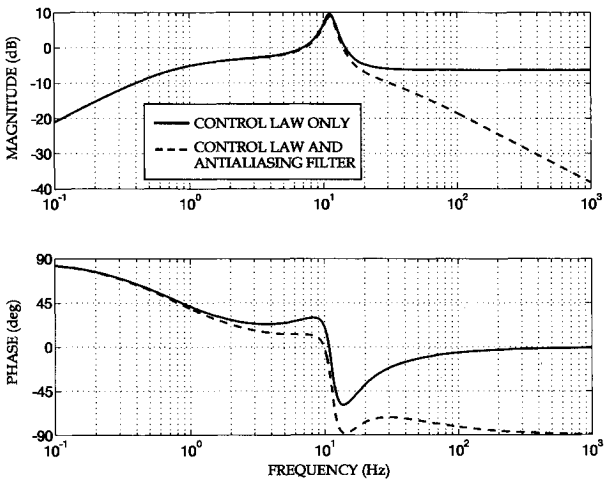

Fig. 3 Control law frequency response (deg/g).

The inverted notch filter characteristic is somewhat more complicated than many of the classical designs used in other flutter suppression studies.[3-5,9-11] Many of the previous designs used first- or second-order filters to adjust the phasing of the counterclockwise loop of the Nyquist plot to ensure an encirclement of the critical point. The loop was already of sufficient size to produce closed-loop stability with the required stability margins without more complicated compensation. This is not the case for the AFW because of the presence of the critical zeros. The counterclockwise loop was "shaped" with the inverted notch filter to provide stability and the required stability margins.

The filter described above was used to suppress symmetric flutter, regardless of whether or not the model was free-to-roll, since the symmetric flutter behavior was independent of whether or not the roll brake was engaged. The same filter parameters were also used to suppress the antisymmetric flutter mode when the roll brake was on. This was possible because of the similarity of the flutter characteristics of the two flutter modes. Only the TEO surface was used in the symmetric control law, whereas both the TEO and TEI surfaces were used in controlling the antisymmetric flutter mode. However, both pairs of trailing-edge control surfaces were driven by the same command signal with a TEI/TEO gain ratio of -0.25. This ratio was chosen to simultaneously maximize gain and phase margins over the range of dynamic pressures.

The FSS control law was designed independently from the rolling maneuver controllers. However, issues associated with simultaneously performing flutter suppression and rapid rolling maneuvers were considered in the FSS design. The washout filter, included in the FSS control law structure to attenuate biases and low-frequency disturbances, provided the required attenuation of low-frequency roll commands. A major concern was the potential for the two controllers to compete for control power when the control surface commands caused the surface deflection or actuator rate limits to be exceeded. If this situation occurred, performance would degrade, and if it occurred at conditions above the open-loop flutter point for sufficiently long periods of time, flutter would occur.

Deflection limits were placed on the roll controller commands so that there would be sufficient control deflection capability for the FSS controller to perform its flight critical function. Rate limits could not be imposed in a similar manner, however, due to controller software and hardware constraints. As a result, the potential for rate limiting had to be addressed in the design of the FSS control law.

The approach to assess possible interactions was to consider the impact of a worst-case scenario. The FSS control laws used the TEO surfaces as their primary control. The deflection limits imposed on the rolling maneuver controller commands were ± 10 deg. A typical rolling maneuver involved initiating a roll, sustaining it for a short period, and then stopping in less than 1.0 s from the time of initiation. Based on these factors, a worst-case roll command was chosen to be a 10-deg doublet to the TEO surface with a period of 1.0 s.

A simulation of the AFW wind-tunnel model was driven by the roll doublet and wind-tunnel turbulence while the FSS controller was operating at a dynamic pressure of 300 psf. During the simulated roll maneuver some rate limiting occurred. However, the limiting only affected one side of the AFW at each instant. When the roll command required maximum control surface rate (to initiate or stop the roll), one TEO surface moved up and the other moved down at the rate limit. The symmetric flutter suppression controller simultaneously commanded control deflections that caused both TEO control surfaces to move in the same direction. Therefore, the side that was commanded by both controllers to move in the same direction experienced rate limiting, but the other surface operated below the rate limit. The flutter suppression control law never became completely ineffective due to rate limiting, but lost some effectiveness. In effect, some of the gain margin was "used up" during the period of rate limiting. The FSS controller maintained system stability subject to the simulated worst-case roll doublet.

Controller Performance and Robustness

Predicted Closed-Loop Performance

The predicted effect of applying the FSS controller to the nominal AFW wind-tunnel model is represented by the symmetric closed-loop dynamic pressure root loci presented in Fig. 4. The FSS control laws were predicted to simultaneously stabilize both the symmetric and antisymmetric flutter modes to dynamic pressures in excess of 325 (over 325 psf for the symmetric mode alone, and over 350 psf for the antisymmetric mode alone). In addition, the control law was able to suppress the primary flutter mode without significantly affecting the higher frequency dynamics. A comparison of the open-loop and closed-loop dynamic pressure root loci[16] shows that the differences are primarily restricted to the flutter region with only slight perturbations of the poles and zeros at higher frequencies.

The predicted control surface activity required to achieve the predicted level of flutter suppression was below the allowable maximum (i.e., 50 deg/s), over the range of dynamic pressure from 100 to 300 psf for both the fixed-in-roll and free-to-roll cases. These predictions were based on estimates of wind-tunnel turbulence modeled using a Dryden spectrum.

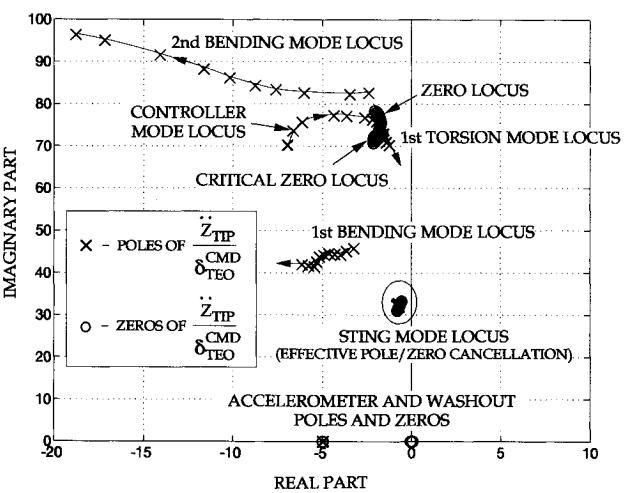

Fig. 4 Close-up of symmetric dynamic pressure root loci: closed-loop (dynamic pressure range: 100–350 psf, 25-psf intervals).

Robustness

Predictions of the symmetric and antisymmetric gain and phase margins for two sets of linear models are presented in Fig. 5. The two models consisted of slightly different aerodynamic representations. Model 1 had a single aerodynamic lag associated with each structural mode to characterize unsteady effects. Model 2 had four aerodynamic lags and slightly different in vacuo vibration frequencies. The stability margins were computed by breaking the loop at the input to the controller (i.e., at the sensor channel).

The symmetric control law was single-input/single-output, and so the gain and phase margins are accurate measures of overall system robustness. The antisymmetric control law was single-input/multi-output, and so the single-loop gain and phase margins were potentially nonconservative since robustness for multivariable systems should be assessed at both the plant input and plant output and by breaking multiple loops simultaneously.[24] However, since the control law was implemented so that both the control surfaces received the same command (to within a constant factor of -0.25), and the uncertainties associated with the two control surface pairs are highly dependent, the effective single-loop margins were deemed acceptable. More general multivariable stability margin measures (e.g., minimum singular value of the inverse return difference matrix at the plant input) were conservative in this instance. This is the case because the multivariable stability margins reflect sensitivity to complex valued perturbations injected independently into each (input or output) channel.[24]

Both the symmetric and antisymmetric controllers satisfied the ± 4 dB gain margin specifications over a range of dynamic pressures from 100 to 325 psf. The ± 30 deg phase margin specifications were satisfied over a range of dynamic pressures from 100 to 350 psf with one exception; at dynamic pressures between 300–350 psf the negative symmetric phase margins were within 1 deg of the specification.

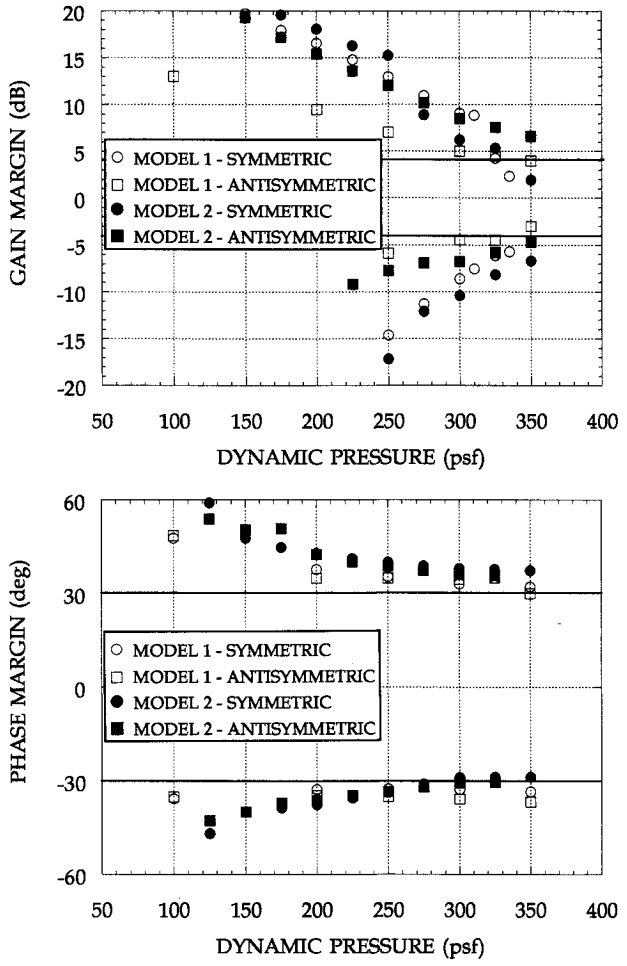

Fig. 5 Predicted stability margins.

Sensitivity analysis was performed to further address the impact of uncertainties in control surface effectiveness and aeroelastic modal frequencies. The nonlinear simulation model was used to evaluate the stability of the closed-loop system at a dynamic pressure of 300 psf, subject to simultaneous variations in the frequencies of the two modes involved in the flutter mechanism (first bending and first torsion in Fig. 2) and variations in control effectiveness. This was accomplished by separating the aerodynamic stiffness terms from the in vacuo vibration frequencies and perturbing the aerodynamic stiffnesses by $\pm 10\%$. Variations in control effectiveness were approximated by varying control law gain by ± 4 dB.

The results of this analysis applied to the symmetric dynamics, presented in Table 1, suggest that the symmetric controller was sensitive to simultaneous increase in the bending mode frequency and decrease in the torsion mode frequency as indicated by the matrix elements in Table 1. The controller was otherwise predicted to be robust to errors in the critical aeroelastic mode frequencies and control effectiveness.

Wind-Tunnel Test Results

Two wind-tunnel tests were performed using the FSS controller. The first test was aimed at performing plant estimation, flutter clearance tests, and validating the performance of active flutter suppression controllers and rolling maneuver controllers individually. The second test was aimed at more extensive flutter suppression and rolling maneuver control tests, and validating the combination of flutter suppression and rolling maneuver control.

The FSS control law succeeded in simultaneously suppressing two flutter modes (symmetric and antisymmetric) when the vehicle was fixed-in-roll and suppressing the single symmetric flutter mode when the vehicle was free-to-roll. The flutter dynamic pressure was increased by over 24% when the model was fixed-in-roll, and by over 23% when the model was free-to-roll. The other flutter suppression control laws tested had very similar levels of performance.[12,13,25]

In the fixed-in-roll case, oscillatory structural deflections caused loads that were in excess of preset safety limits. The excessive loads occurred at a dynamic pressure of 272 psf, at which point testing was curtailed. Extrapolation of the experimental data suggests that the controller would be able to maintain stability to dynamic pressures near 300 psf.

Table 1 Sensitivity to aeroelastic frequency and control effectiveness variations, symmetric mode (dynamic pressure = 300 psf)

ω_b \ ω_τ	-10%	Nom.	$+10\%$
	ΔGain = -4 dB		
-10%	S^a	S	S
Nom.	S	S	S
$+10\%$	U	U	S
	ΔGain = 0 dB		
-10%	S	S	S
Nom.	S	S	S
$+10\%$	U	S	S
	ΔGain = $+4$ dB		
-10%	S	S	S
Nom.	S	S	S
$+10\%$	U	S	S

[a]Indicates actual model errors identified during the test.

ω_b = bending mode frequency.
ω_τ = torsion mode frequency
S = stable.
U = unstable.

In the free-to-roll case the maximum dynamic pressure of the wind tunnel (290 psf) was reached making further increases in dynamic pressure impossible. Extrapolation of the experimental data indicated that the dynamic pressure could have been increased to approximately 330 psf before instability would occur. However, the safety limits would likely be exceeded before the stability limit could be attained, as was the case when the model was fixed-in-roll.

The control activity that was required to achieve the demonstrated levels of flutter suppression was less than half the design requirement. The peak rms control rate was less than 15 deg/s, which is well below the predicted level of approximately 54 deg/s. It is possible that higher gains could have been used to exploit the available control activity and improve controller performance. However, the gain values were based more on obtaining uniform stability margins than on limiting control activity, and higher gains would also have led to smaller stability margins.

Another measure of performance of the FSS controller was the level of stability indicated by the Nyquist plot depicted in Fig. 6. This plot corresponds to the symmetric AFW/FSS loop transfer function at a dynamic pressure of 250 psf, which is beyond open-loop flutter. Plots based on both the experimental data and the mathematical model of the AFW/FSS are shown for comparison. The plot based on experimental data was obtained using the method described in Refs. 26 and 27.

The jagged nature of the experimentally derived plot is due to the fact that the counterclockwise encirclement of the critical point, -1, occurs over a very small range of frequencies. Even though the frequency resolution is quite high, the number of data points defining the loop are relatively few. However, the encirclement is clearly evident and shows good agreement with the prediction. The primary discrepancy between the predicted and actual results can be attributed to a phase shift due to additional time delay of approximately one-half sample period, 0.0025 s, included in the analysis of the FSS. The gain margins were well in excess of the ± 4 dB required, and although the positive phase margin exceeded the requirement, the negative phase margin was slightly smaller than -30 deg.

The FSS controller was combined with a rolling maneuver controller[28] to demonstrate the ability to perform flutter suppression while performing rapid rolling maneuvers. The test involved performing the rolling maneuvers over a range of dynamic pressures both below and above flutter. At a dynamic pressure of 275 psf (39 psf beyond open-loop flutter), the rolling maneuver controller accomplished a 90-deg roll, starting from rest, in less than 0.5 s. The flutter suppression controller had no difficulty maintaining stability during the rolling maneuver, and the control activity and vehicle responses indicated no significant differences between the FSS performance in either steady or maneuvering conditions.

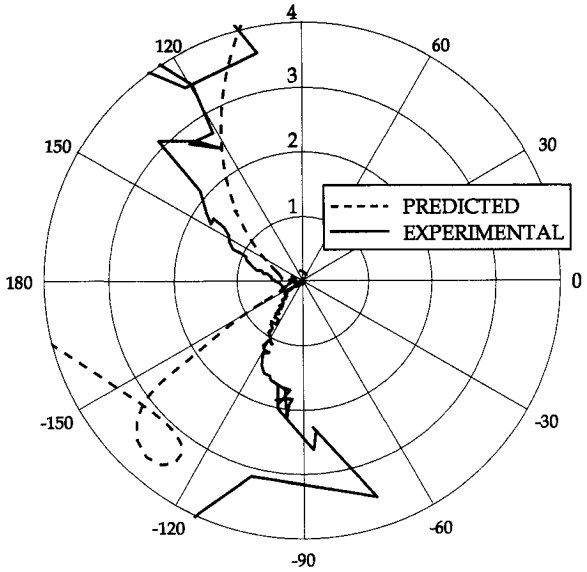

Fig. 6 Nyquist plot of $\ddot{Z}_{TIP}$ (g)—symmetric, 250 psf.

Modeling Errors

Plant identification was performed during both wind-tunnel tests. The experimentally determined open-loop flutter dynamic pressures were 235 and 219 psf for the symmetric (fixed- and free-to-roll) and antisymmetric (fixed-in-roll) modes, respectively (somewhat lower than the predicted values presented previously). The experimentally determined flutter frequencies were 9.6 and 9.1 Hz for the symmetric and antisymmetric modes, respectively. The predicted flutter frequencies, stated previously, were somewhat higher. The errors in the predicted flutter frequencies were 16.7 and 19.8% for the symmetric and antisymmetric modes, respectively.

Transfer functions for key input-output pairs at subcritical dynamic pressures (i.e., below flutter) were determined prior to closing the loop with the FSS controller, and again after the control loops were closed to evaluate the accuracy of the model. Figures 7 and 8 present two representative transfer function plots for the tip accelerometer response due to antisymmetric TEO control surface deflection with the model fixed-in-roll. Figure 7 corresponds to a dynamic pressure of 150 psf, which is well below the flutter dynamic pressure. The

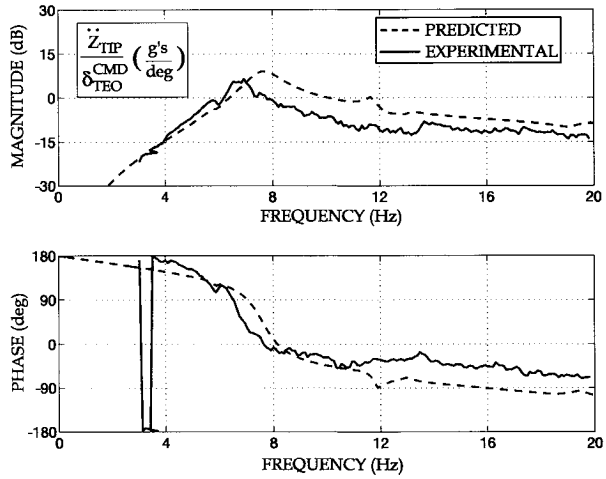

Fig. 7 Open-loop frequency response—antisymmetric, fixed-in-roll (dynamic pressure = 150 psf).

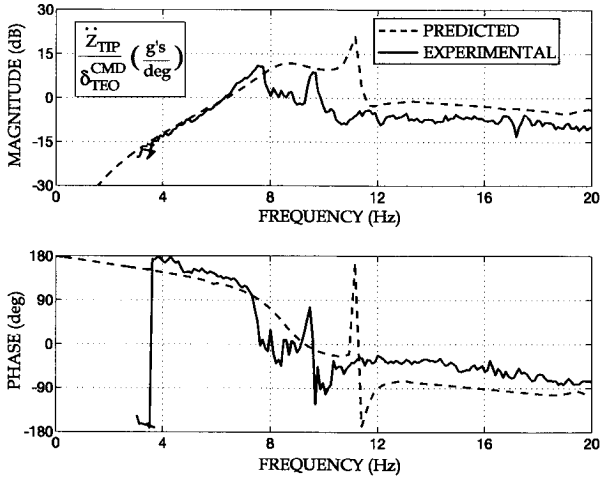

Fig. 8 Open-loop frequency response—antisymmetric, fixed-in-roll (dynamic pressure = 225 psf).

plot in Fig. 8 corresponds to a dynamic pressure of 225 psf, which is very near the actual flutter dynamic pressure.

In both cases there is general agreement between the shapes of the predicted and true responses, however, there are also notable differences. One of the most notable differences is the shift in the frequencies of the key aeroelastic modes. This results in the flutter frequency errors discussed previously. Similar discrepancies occurred for the symmetric responses.[14]

Another difference between the analytical and experimental frequency responses in Figs. 7 and 8 are the peak magnitudes. The differences in the range of frequencies near flutter vary from 3 to 10 dB over a range of dynamic pressure from 150 psf to 225 psf. As a result, the actual control effectiveness in the antisymmetric flutter frequency range was considerably less than was predicted.

Fortunately, the FSS controller was robust to errors in both control effectiveness and aeroelastic mode frequencies, as shown in the results from the sensitivity analyses. The entry in Table 1, indicated by superscript "a," corresponds to simultaneous reduction in control effectiveness and reduction in bending and torsion mode aeroelastic frequencies.

Concluding Remarks

One objective of the AFW program was to apply multivariable control methods to the flutter suppression problem. It was found, however, that a simple low-order, single-input/single-output control law could be designed using traditional methods with performance similar to more sophisticated multivariable optimization-based control laws. In addition, the classical controller was successful without any modifications or tuning based on test data, which was not the case for the optimization-based control laws.

The control law was shown to simultaneously suppress two clean wing flutter modes in steady flight and a single flutter mode while performing rapid rolling maneuvers representative of high-performance military aircraft. These accomplishments were achieved despite modeling errors in control effectiveness, flutter frequency, and flutter dynamic pressure in the design model, which nevertheless accurately characterized the flutter mechanism.

The application of traditional, graphical design tools to the flutter suppression problem was greatly aided by the availability of computer-aided design tools that allow large, complex mathematical models of a dynamical system to be easily manipulated and analyzed. The power of the graphical methods like root locus and Nyquist plots to identify important features of the system dynamics (e.g., pole and zero locations, frequency separations, pole/zero cancellations, stability margins, etc.), combined with the speed and ease-of-use afforded by computer-aided design tools, was a key to the success of this AFW FSS control law.

While it may not always be feasible to solve a flutter suppression problem with a single-input/single-output feedback structure, the insight and perspectives available through the traditional graphical analysis tools should be exploited whenever possible. These tools complement the more sophisticated optimization-based methods that have the potential to mask key features of the dynamics and produce counterintuitive solutions. The graphical methods (and their multivariable extensions) can be used to provide an alternate perspective, as a point of reference for other designs, or even as a starting point for control law design using alternate methods.

Acknowledgment

The authors wish to express their appreciation to Matthew J. Cummings for his efforts in obtaining the numerical results presented herein.

References

[1]Miller, G. D., "Active Flexible Wing (AFW) Technology," Air Force Wright Aeronautical Labs., AFWAL-TR-87-3096, Feb. 1988.

[2]Perry, B., Cole, S. R., and Miller, G. D., "A Summary of the Active Flexible Wing Program," AIAA Paper 92-2080, April 1992.

[3]Triplett, W. E., Kappus, H. F., and Landy, R. J., "Active Flutter Control," AIAA Paper 73-194, Jan. 1973.

[4]Redd, L. T., Gilman, J., Jr., Cooley, D. E., and Sevart, F. D., "Wind-Tunnel Investigation of a B-52 Model Flutter Suppression System," *Journal of Aircraft*, Vol. 11, No. 11, 1974, pp. 659–663.

[5]Roger, K. L., and Hodges, G. E., "Active Flutter Suppression—A Flight Test Demonstration," *Journal of Aircraft*, Vol. 12, No. 6, 1975, pp. 551–556.

[6]Newsom, J. R., "Synthesis of Active Flutter Suppression Systems Using Optimal Control Theory," AIAA Paper 78-1270, Aug. 1978.

[7]Sandford, M. D., Abel, I., and Gray, D. L., "Development and Demonstration of a Flutter-Suppression System Using Active Controls," NASA TR R-450, Dec. 1975.

[8]Adams, W. M., and Tiffany, S. H., "Design of a Candidate Flutter Suppression Control Law for DAST ARW-2," NASA TM 86257, July 1984.

[9]Peloubet, R. P., Jr., Haller, R. L., and Bolding, R. M., "Recent Developments in the F-16 Flutter Suppression with Active Control Program," *Journal of Aircraft*, Vol. 21, No. 9, 1984, pp. 716–721.

[10]Van Gelder, P. A., "NLR Experience in the Application of Active Flutter Suppression and Gust Load Alleviation, Applied to a Wind-Tunnel Model," Second International Symposium on Aeroelasticity and Structural Dynamics, Aachen, Germany, April 1985, pp. 320–329.

[11]Schmidt, D. K., and Chen, T. K., "Frequency Domain Synthesis of a Robust Flutter Control Law," *Journal of Guidance and Control*, Vol. 9, No. 3, 1986, pp. 346–351.

[12]Christhilf, D. M., and Adams, W. M., Jr., "Multifunction Tests of a Frequency Domain Based Flutter Suppression System," AIAA Paper 92-2096, April 1992.

[13]Mukhopadhyay, V., "Flutter Suppression Digital Control Law Design and Testing for the AFW Wind-Tunnel Model," AIAA Paper 92-2095, April 1992.

[14]Waszak, M. R., and Srinathkumar, S., "Design and Experimental Validation of a Flutter Suppression Controller for the Active Flexible Wing," NASA TM-4381, Aug. 1992.

[15]Adams, W. M., Christhilf, D. M., Waszak, M. R., Mukhopadhyay, V., and Srinathkumar, S., "Design, Test, and Evaluation of Three Active Flutter Suppression Controllers," NASA TM-4338, Oct. 1992.

[16]Waszak, M. R., and Srinathkumar, S., "Flutter Suppression for the Active Flexible Wing: Control System Design and Experimental Validation," AIAA Paper 92-2097, April 1992.

[17]Srinathkumar, S., and Waszak, M. R., "Active Flutter Suppression Using 'Dipole' Filters," NASA TM-107594, Sept. 1992.

[18]Hoadley, S. T., and McGraw, S. M., "The Multiple-Function Multi-Input/Multi-Output Digital Controller System for the AFW Wind-Tunnel Model," AIAA Paper 92-2083, April 1992.

[19]Buttrill, C. S., and Houck, J. A., "Hot-Bench Simulation of the Active Flexible Wing Wind-Tunnel Model," AIAA Paper 90-3121, Sept. 1990.

[20]Buttrill, C. S., Bacon, B. J., Heeg, J., Houck, J. A., and Wood, D., "Simulation and Model Reduction for the AFW Program," AIAA Paper 92-2081, April 1992.

[21]Tiffany, S. H., and Adams, W. M., Jr., "Nonlinear Programming Extensions to Rational Function Approximation Methods for Unsteady Aerodynamic Forces," NASA TP-2776, July 1988.

[22]Bisplinghoff, R. L., and Ashley, H., *Principles of Aeroelasticity*, Dover, New York, 1975.

[23]Waszak, M. R., and Buttrill, C. S., "Design of an Active Flutter Suppression System for the Active Flexible Wing," AIAA Paper 91-3111, Sept. 1991.

[24]Maciejowski, J. M., *Multivariable Feedback Design*, Addison-Wesley, Reading, MA, 1989.

[25]Klepl, M. J., "A Flutter Suppression System Using Strain Gages Applied to Active Flexible Wing Technology: Design and Test," AIAA Paper 92-2098, April 1992.

[26]Pototzky, A. S., Wieseman, C. D., Hoadley, S. T., and Mukhopadhyay, V., "Development and Testing of Methodology for Evaluating the Performance of Multi-Input/Multi-Output Digital Control Systems," NASA TM 102704, Aug. 1990.

[27]Wieseman, C. D., Hoadley, S. T., and McGraw, S. M., "On-Line Analysis Capabilities Developed to Support the AFW Wind-Tunnel Tests," AIAA Paper 92-2084, April 1992.

[28]Moore, D. B., "Maneuver Load Control Using Optimized Feedforward Commands," AIAA Paper 92-2100, April 1992.